Journal of Marine Science and Engineering

Article

Design of Underwater Wireless Power Transmission System Based on Inductive Coupling

Tianchu Luo [1,2,*] and Shaowei Zhang [1,*]

[1] Institute of Deep-Sea Science and Engineering, Chinese Academy of Sciences, Sanya 572000, China
[2] College of Materials Science and Opto-Electronic Technology, University of Chinese Academy of Sciences, Beijing 100049, China
[*] Correspondence: tianchuluo@126.com (T.L.); zswsia@126.com (S.Z.)

Abstract: Human exploration of the ocean is inseparable from reliable ocean observation equipment. Wireless power transmission technology can supply power to the receiving end in a non-contact manner, saving complicated cable plugging and unplugging. Due to the conductivity of seawater, a certain amount of eddy current loss will be generated during wireless power transmission, reducing the output power and transmission efficiency. This paper designs a wireless power transmission system suitable for underwater scenes, and in this paper, the operational characteristics of the system are analyzed. At the same time, the transmission capability of the system in the air is studied, and the influence of several key parameters such as resonance frequency on the output power and transmission efficiency is analyzed. On this basis, combined with the calculation method of eddy current loss in seawater, the system transmission efficiency in seawater is calculated, which provides a reference for selecting the operating frequency. Finally, a coupler design scheme that is easy to dock with underwater devices and has a good electromagnetic shielding effect is given, and its transmission capability and performance under misalignment are analyzed through finite element simulation. According to the design plan, a prototype is built and experiments are carried out in air and simulated seawater environments. The experimental results verify the correctness of the theory.

Keywords: underwater wireless power transfer; ocean observation; inductive coupling; eddy current loss; magnetic coupler design

Citation: Luo, T.; Zhang, S. Design of Underwater Wireless Power Transmission System Based on Inductive Coupling. *J. Mar. Sci. Eng.* **2023**, *11*, 1699. https://doi.org/10.3390/jmse11091699

Academic Editor: Dong-Sheng Jeng

Received: 30 July 2023
Revised: 20 August 2023
Accepted: 25 August 2023
Published: 28 August 2023

1. Introduction

Ocean exploration and development are inseparable from reliable underwater electromechanical equipment, such as underwater vehicles, ocean observation buoy systems, etc. Due to the volume and load limitation, the battery capacity of these devices is usually limited. Supplying power for these devices is a fundamental problem in ocean observation. Salvaging the device and replacing the battery requires manual operation, which has high labor costs and low work efficiency. Another way is to use a wet-pluggable connector to charge the device. This method is expensive and has specific potential safety hazards. One of the wireless power transmission technologies, inductively coupled power transfer technology (ICPT), is based on the principle of electromagnetic induction and transmits energy from the transmitter to the load in a non-contact manner. It has been widely used in many fields. Applying it in the underwater field can improve charging safety and reliability, prolong battery life, and effectively solve the power supply problem for underwater equipment.

The research area of the wireless power transmission of underwater vehicles is the most popular and influential field in the application of wireless power transmission in the underwater field [1]. Due to the underwater vehicle's shuttle-shaped structure, the magnetic coupler design is usually combined with the shape of the underwater vehicle and the docking station, and the wireless power transmission system starts to work when the underwater vehicle enters the docking station [2]. Dave Pyle et al. developed a docking station system for providing wireless power supply to the Proteus unmanned underwater vehicle (UUV). When the small aircraft carried by the UUV needs to be charged, it will leave the side compartment of the UUV and enter the docking station for replenishment [3]. Shi et al. propose an optimized structure for a docking system consisting of two large-diameter coaxial coils, one of which is mounted on the aluminum housing of the autonomous underwater vehicle (AUV) and the other on the docking station. This solution solves the problem of radial misalignment between the coils under the impact of water flow, and the installation method of the coils does not affect the external structure of the AUV [4]. Yan et al. propose an arc-shaped improved EE core coupler structure. The primary and secondary are installed on the docking station and the AUV, respectively. Compared with the flat coupler, the arc-shaped coupler is easier to install in the AUV and facilitates alignment, which can reduce magnetic leakage and maximize transmission efficiency [5].

Many sensors are mounted in the ocean observation buoy system, and the battery capacity is limited and inconvenient to replace, limiting the system's flexibility and working time [6]. The wireless power supply for the ocean observation buoy system will solve this problem, which is one of the essential applications of underwater wireless power transmission technology. Due to the unique structure of the buoy system, the wireless power supply system usually adopts the coupler form of a linear coaxial winding transformer [7]. The primary of the coupler is a slender cable, and the secondary is installed at the equipment. This structure facilitates simultaneous power and data transmission to multiple underwater sensors. Yoshioka et al. designed a device to supply power to underwater sensors in the Triangle Trans-Ocean Buoy Network (TRITON). This design uses a mooring steel cable as the primary side magnetic core, and the primary coil is wound around it. The secondary coil and the underwater sensor are housed in a waterproof cylinder. The design facilitates directly using the mooring steel cable as the primary side and has a certain simplicity, but there is a main magnetic flux in this space during the working process, and the large contact area with the seawater will increase the eddy current loss to a certain extent and reduce the transmission efficiency [8]. McGinnis et al. designed an inductively coupled power transfer system for a moored ocean profiler that moves between buoys on the seafloor and a cable platform. The primary of the inductive coupler is fixed to the mooring cable, and the secondary is mounted on the profiler, which supplies power to the battery through a rectifier, both coaxial with the mooring cable. However, this design makes it difficult to clamp and remove the secondary coupler from the mooring cable, which reduces the ease of application of the device [9].

Due to the seawater environment's particularity and the working scene's uniqueness, there are many vital issues and challenges to be solved in the wireless power transmission system that is applied to the seawater [10]. As a transmission medium, seawater has a specific conductivity. When the wireless power transfer system is working, eddy currents will be generated in seawater, which will cause additional power loss at higher frequencies and affect the system's electromagnetic characteristics [11]. Zhou et al. studied the relationship between the frequency, load, and eddy current loss of electromagnetic couplers in air and seawater. They propose an analytical method for calculating the eddy current loss generated by seawater. However, the method in this paper does not provide a theoretical calculation method for the optimal frequency, but illustrates it through the experimental results of the transmission efficiency corresponding to the switching frequency under different load conditions [12]. Zhang et al. established a systematic mathematical model for the seawater environment through Maxwell's equations, obtained an approximate formula for calculating eddy current loss through series expansion, and analyzed the relationship between eddy current loss and coil radius, resonance frequency, transmission distance, and other factors [13]. Askari et al. studied the influence of seawater's conductivity on the ICPT system's transmission efficiency through experiments. The experiments were carried out at four different resonance frequencies. Their experimental results showed that the transmission efficiency between seawater and air would significantly differ after exceeding 20 kHz [14]. The above work derives the calculation method of seawater eddy current loss or only measures the transmission efficiency of ICPT in seawater through experiments and does not theoretically combine the calculation of seawater eddy current loss with the system transmission efficiency calculation method, which cannot provide a reliable reference for the selection of operating frequency. The application designed in this paper is oriented to small and medium power underwater observation equipment, such as sensor nodes on the buoy system. The developed system has high transmission efficiency. Compared with historical work, this paper makes a complete analysis of three important parameters (resonant frequency, load, and coupling coefficient) that affect system performance. In practical applications, system parameters can be adjusted according to power or efficiency preferences. At the same time, this research fills the gap in the field of research on small- and medium-scale power transmission systems.

The remainder of this paper is organized as follows: the second section discusses the circuit topology suitable for underwater scenes, analyzes the operational characteristics of the system, and deduces the operational characteristics of the system circuit topology; the third section studies the overall output power and transmission efficiency of the system, combining the calculation method of eddy current loss analyzes and calculates the output power and output efficiency of the system in the seawater; the fourth section chooses a coupler structure with high transmission capacity and low electromagnetic interference; the fifth section introduces the prototype made based on the design scheme and the experimental platform, and experiments have been conducted to verify the feasibility and correctness of the theoretical scheme.

2. Principle Design of Inductive Coupling Circuit

The underwater wireless power transmission system based on inductive coupling consists of three parts: the transmitter, the receiver, and the magnetic coupler. The transmitter includes a DC power supply, a DC–AC converter, and a transmitter resonance compensation network. The receiver includes a receiver resonance compensation network, an AC–DC converter and filter circuit, and a load (electrical equipment). The magnetic coupler is an electromagnetic energy conversion unit to connect the transmitter and the receiver. A block diagram of the entire system is shown in Figure 1.

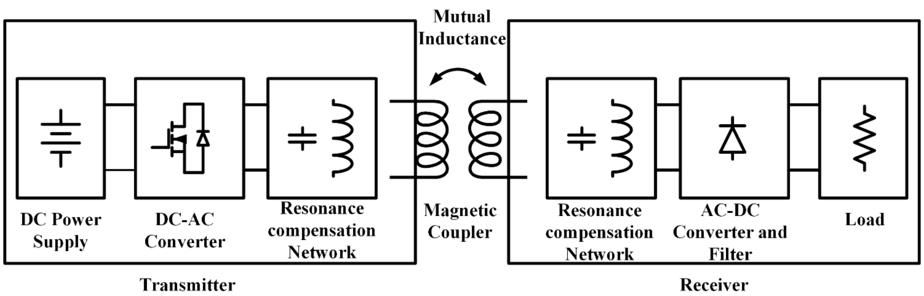

Figure 1. System structure diagram.

The circuit model of the wireless power transfer system with SS compensation network is shown in Figure 2. Among them, U_d is the input DC voltage source; $Q_1 \sim Q_4$ is the four power MOSFET switch tubes which constitutes a full-bridge inverter and converts the input DC power to AC power; L_p and L_s are the self-inductance of the system transmitting coil and receiving coil, respectively, and the corresponding coil internal resistances are R_{Lp} and R_{Ls}, respectively; C_p and C_s are the series compensation capacitors of the transmitting coil and receiving coil, respectively; M is the mutual inductance between the transmitting coil and the receiving coil; the four rectifier diodes $D_1 \sim D_4$ together form a full-bridge uncontrolled rectifier circuit, which rectifies the received AC power into DC power; C_F is the output filter capacitor, and R_L is the equivalent load; i_{in}, i_p, and i_s are the output current of the inverter, the current of the transmitting coil, and the current of the receiving coil, respectively.

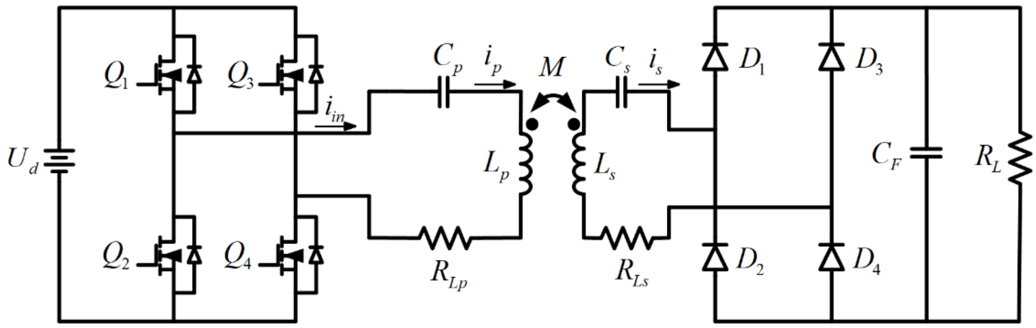

Figure 2. Wireless power transfer system with SS compensation network.

In order to facilitate an analysis of the operational characteristics of the circuit topology, the following approximation is made: In the actual system, the on-resistance of the MOSFET and the diode is much smaller than the internal resistance of the coil used, so the on-resistance of the MOSFET and the diode is ignored. The output voltage of the full-bridge inverter is equivalent to the effective value of the fundamental voltage, ignoring the high-frequency harmonic components, and according to the Fourier series, the effective value of the fundamental wave can be obtained as $U_{in} = \left(2\sqrt{2}/\pi\right)U_d$; assuming that the output filter capacitor is large and the output voltage is constant, the rectifier filter circuit at the receiver can be equivalent to a pure resistive load $R_e = \pi^2 R_L/8$. The equivalent circuit model obtained after approximation is shown in Figure 3a. Let the switching angular frequency of the inverter be ω, the total impedance of the receiver circuit be Z_s, and the reflected impedance of the receiver to the transmitter be Z_r. The notations involved in the model are summarized in Table 1. The equivalent circuits of the transmitter and the receiver of the system can be represented as shown in Figure 3b,c, respectively:

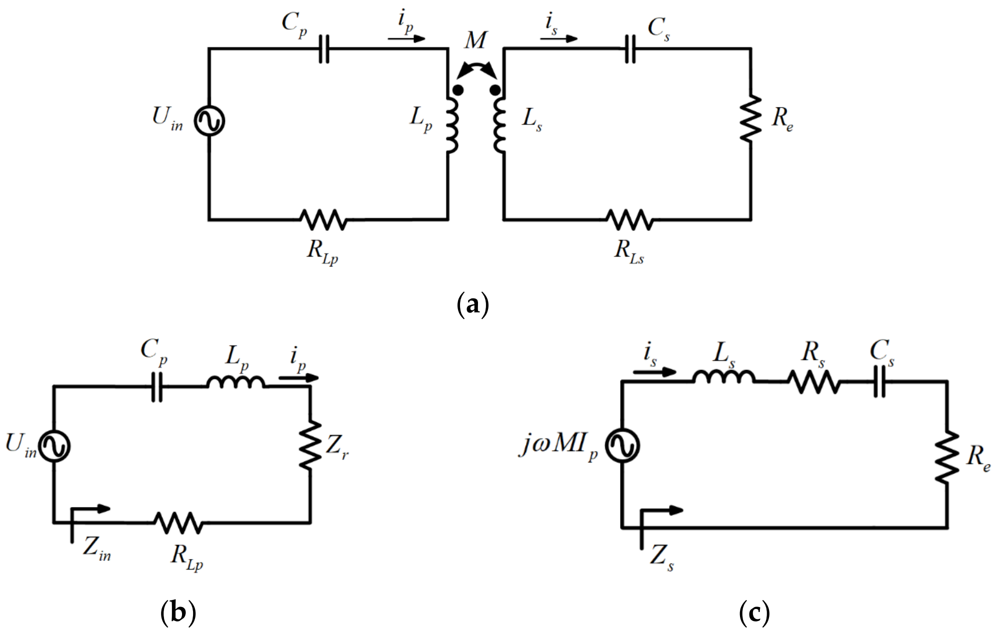

Figure 3. Wireless power transfer system with SS compensation network: (**a**) equivalent circuit model; (**b**) transmitter equivalent circuit; (**c**) receiver equivalent circuit.

Table 1. Notation.

Notation	Description
U_{in}	RMS value of input voltage
L_p, L_s	Self-inductance of each coil
C_p, C_s	Compensation capacitance for each side
ω	Transmission frequency
M	Mutual inductance
R_e	Equivalent load
Z_s	Total impedance of the receiver
Z_r	Reflected impedance of the receiver
Z_{in}	Total input impedance
$\dot{I}_p$, $\dot{I}_s$	Coil current in transmitter and receiver
$\dot{U}_o$	Output voltage
G_v	Output voltage gain

During the working process of the circuit, to reduce the reactive power in the transmission process and improve the transmission efficiency, it is necessary to configure the system to reach a resonance state. Among them, the coil inductance L_p and capacitance C_p form a resonant circuit in the transmitter. In the receiver, the coil inductance L_s and capacitance C_s form a resonant circuit, and the two resonant circuits have the same resonant frequency, which has the following relationship:

$$\begin{cases} \omega L_p = \frac{1}{\omega C_p} \\ \omega L_s = \frac{1}{\omega C_s} \end{cases} \tag{1}$$

The total impedance Z_s of the receiver, the reflected impedance Z_r of the receiver to the transmitter, and the total input impedance Z_{in} can be expressed as follows:

$$\begin{cases} Z_s = R_{Ls} + R_e \\ Z_r = \frac{(\omega M)^2}{R_{Ls}+R_e} \\ Z_{in} = R_{Lp} + \frac{(\omega M)^2}{R_{Ls}+R_e} \end{cases} \tag{2}$$

In the process of wireless power transmission, in order to obtain high transmission capacity, it is necessary to configure a coil with a high quality factor and a small internal resistance. When ignoring the internal resistance in the coil, Formula (2) can be expressed as follows:

$$\begin{cases} Z_s = R_e \\ Z_r = \frac{(\omega M)^2}{R_e} \\ Z_{in} = \frac{(\omega M)^2}{R_e} \end{cases} \tag{3}$$

The expressions for the coil currents at the transmitter and receiver can be expressed as follows:

$$\begin{cases} \dot{I}_p = \frac{\dot{U}_{in} R_e}{(\omega M)^2} \\ \dot{I}_s = \frac{j\dot{U}_{in}}{\omega M} \end{cases} \tag{4}$$

The system output voltage can be expressed as follows:

$$\dot{U}_o = \dot{I}_s R_e = \frac{j\dot{U}_{in} R_e}{\omega M} \tag{5}$$

The output voltage gain can be expressed as follows:

$$G_v(\omega) = \left| \frac{\dot{U}_o}{\dot{U}_{in}} \right| = \left| \frac{jR_e}{\omega M} \right| \tag{6}$$

According to the above derivation and analysis, it can be concluded that the wireless power transmission system of the SS type resonance compensation network has the following characteristics: (1) When working at the resonant frequency, the output current at the receiver I_s is only related to the system input voltage U_{in} and has an output characteristic independent of the load. It can realize constant current output without adding additional control circuits and is not disturbed by load changes. (2) The expression of the resonant capacitance $C_p = \frac{1}{\omega^2 L_p}$ at the transmitter has nothing to do with the mutual inductance M and the load R_e. When the impact of the water flow causes dislocation between the couplers, the change in the parameters will not affect the resonance state of the transmitter. (3) The imaginary part of the reflected impedance Z_r is zero, the input voltage U_{in} and the input current (transmitting coil current) I_p have the same phase, the system has a unit power factor input characteristic, and the reactive power is low.

It can be seen that the wireless power transmission system of the SS type resonant compensation network has certain advantages when applied to the power supply of underwater equipment. While having high efficiency, it also has specific stability under the condition of dislocation interference in the environment. It should be noted that no-load at the receiver is not allowed in the SS topology system. It can be seen from Formula (4) that when the mutual inductance between the two coils approaches zero, the coil current at the transmitter will approach infinity and rise rapidly. High current will cause circuit damage. Therefore, in the design process of the actual system, care should be taken to avoid no load at the receiver, and the software program should be set to stop the converter at the transmitter when the current is detected to be too high.

3. System Performance Analysis

3.1. Analysis of System Output Capability in Air

For wireless power transmission systems, output power and transmission efficiency are essential indicators for evaluating system output capabilities. In the usual land air transmission environment, the output power and transmission efficiency of the wireless power transmission system are mainly related to the coupling coefficient, transmission distance, resonant frequency, and impedance in the coil and circuit components, and the air between the couplers as the transmission medium has little effect on the transmission efficiency. The difference is that, as the transmission medium, seawater has a larger relative permittivity and higher electrical conductivity than air, and the loss generated during the transmission cannot be ignored. This section first calculates and analyzes the system's output power and transmission efficiency in the air, which provides a basis for the analysis of the output capability in the seawater in the following section.

In air, the output power can be expressed as follows:

$$P_{out\_air} = \frac{U_o^2}{R_e} = \left| \frac{j\omega M \dot{U}_{in} R_e}{R_{Lp}(R_{Ls} + R_e) + (\omega M)^2} \right|^2 \frac{1}{R_e} \tag{7}$$

The total system input power can be expressed as follows:

$$P_{in\_total} = \frac{U_{in}^2}{|Z_{in}|} = \frac{U_{in}^2}{\left| R_{Lp} + \frac{(\omega M)^2}{R_{Ls} + R_e} \right|} \tag{8}$$

Among them, except for the part of the total input power that is converted into the power shared by the load, the remaining part is converted into the power loss on the circuit and the power loss on the coil. Then, the transmission efficiency can be expressed as follows:

$$\eta_{air} = \frac{P_{out\_air}}{P_{in\_total}} = \frac{\omega^2 M^2 R_e}{\left(R_{Lp} + R_e\right)\left(\omega^2 M^2 + R_{Lp}^2 + R_{Lp} R_e\right)} \times 100\% \tag{9}$$

In the following, the relationship of several important variables—load resistance, resonant frequency to output power, and transfer efficiency—is analyzed for a wireless power transfer system with a defined electromagnetic coupler. Based on the transmission power level of this design and referring to hardware design experience, the following parameters are set as follows: $L_p = L_s = 8.7$ µH, $R_{Lp} = R_{Ls} = 0.1\Omega$, $U_d = 24$ V.

Under several groups of different resonant frequencies f, the output power P_{out} and transmission efficiency η vary with the load resistance R_e, as shown in Figure 4a,b ($M = 6$ µH). It can be seen that, for any resonant frequency, the output power has a tendency to rise first to reach the maximum value and then decrease with the increase in the load. However, the corresponding optimal load values are different under different frequencies, and the lower resonant frequencies correspond to lower optimum load values. For the transmission efficiency, the curves at different resonance frequencies quickly reach the maximum value and then slowly decrease with the increase in the load, where a higher resonance frequency corresponds to a higher transmission efficiency. It is worth noting that the optimal load values corresponding to the output power and transmission efficiency at the same resonant frequency are not in the same range, which shows that a system cannot satisfy the maximum output power and transmission efficiency simultaneously. The load value needs to be selected according to the preference for the two indicators.

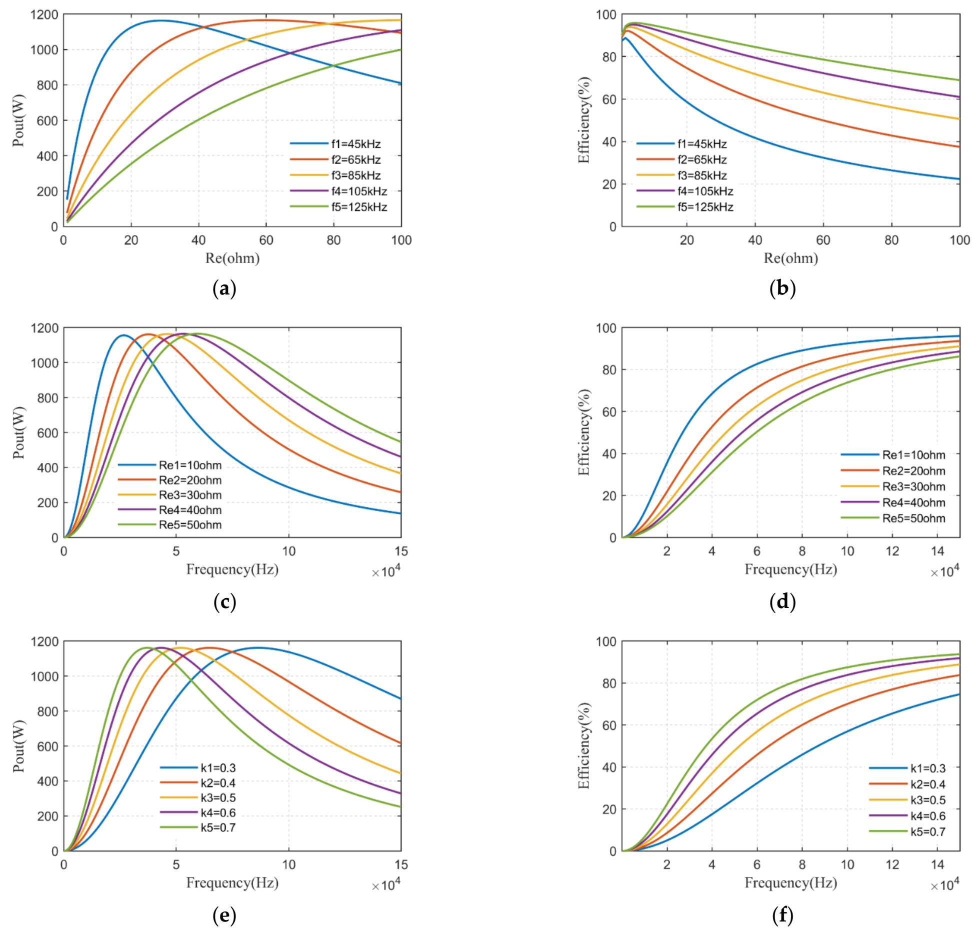

Figure 4. Trends of output power and transmission efficiency as a function of system parameters: (**a**) output power versus load for different resonant frequencies; (**b**) transmission efficiency versus load for different resonant frequencies; (**c**) output power versus resonance frequency for different loads; (**d**) transmission efficiency versus resonance frequency for different loads; (**e**) output power versus resonance frequency for different coupling coefficients; (**f**) transmission efficiency versus resonance frequency for different coupling coefficients.

Under several groups of different load resistance values R_e, the output power P_{out} and the transmission efficiency η vary with the resonant frequency f, as shown in Figure 4c,d ($M = 6$ μH). It can be seen that the output power curves under different loads first rise to the highest point and then decrease with the increase in the resonance frequency. The optimal frequency corresponding to the lower load is lower, but the maximum output power value that can be achieved under different loads is the same. For transmission efficiency, the curves under different loads all have a rising trend with the increase in the resonance frequency, and the load with the lower resistance value in several groups of loads can obtain higher transmission efficiency. For the same system with other parameters fixed, the optimal resonant frequency value of output power and transmission efficiency cannot take the same value. It can be seen that, when the output power in Figure 4c reaches the highest value, the transmission efficiency at this frequency in Figure 4d has not yet reached reach the optimum value. Therefore, comprehensive care and consideration should be taken when selecting the system frequency, that is, to ensure a certain output capability and at the same time, let the system work at a better transmission efficiency.

Under several groups of different coupling coefficients k, the output power P_{out} and transmission efficiency η vary with the resonance frequency f, as shown in Figure 4e,f ($R_e = 20\Omega$). The size of the coupling coefficient is related to the degree of inductive coupling of the system, and the higher the coupling coefficient, the stronger the transmission capacity of the system. It can be seen from Figure 4e that the output power curve corresponding to the highest coupling coefficient first reaches the maximum value, while the curve corresponding to the lower coupling coefficient can reach the same maximum output power through compensation of high resonance frequency. It can be seen from Figure 4f that the greater the coupling coefficient of the system, the higher the corresponding transmission efficiency, which also verifies that the better the degree of inductive coupling, the less magnetic flux leakage between couplers, and the less loss generated.

The above analysis shows that the output power and output efficiency can reach ideal values under certain conditions under the configuration of load resistance, resonance frequency, and coupling coefficient. Nevertheless, at the same time, each parameter cannot meet the optimal solution of power and efficiency simultaneously, and the parameters need to be determined reasonably according to the system performance index. The above analysis has laid the foundation for the subsequent performance analysis in seawater and is an essential basis for designing the system hardware circuit.

3.2. System Output Capability Analysis in Seawater

In seawater, the electrical parameters of seawater as a transmission medium are quite different from those of air, specifically manifested as having a larger relative permittivity ($\varepsilon_r = 81$) and higher conductivity ($\sigma = 4S/m$). During the system's working process, the high-frequency alternating magnetic field formed between the coils of the coupler will induce an eddy electric field in seawater, which will cause eddy current loss and reduce transmission efficiency. Therefore, it is necessary to calculate and analyze the power loss generated in seawater.

The equivalent model of the system in air is shown in Figure 3, and the transmission model in seawater can be based on the equivalent model in air and improved according to the characteristics of the seawater. In the air environment, the loss of the system comes from the impedance in the circuit that consumes electrical energy, which is converted into heat loss. The eddy current loss in seawater also comes from the induction of electric energy converted into heat, so seawater can be regarded as a circuit with specific impedance characteristics, equivalent to the system circuit, as shown in Figure 5.

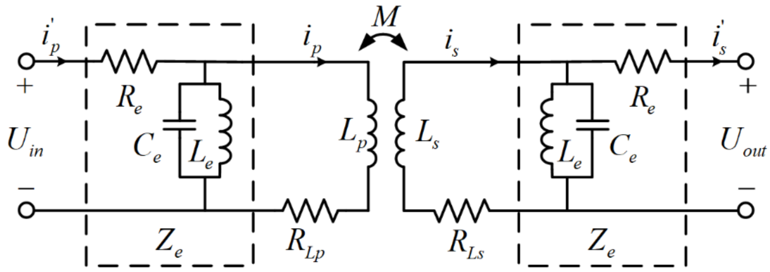

Figure 5. Equivalent transport model in seawater environment.

R_e, C_e, L_e are equivalent resistance, equivalent capacitance, and equivalent inductance, respectively, constituting the equivalent impedance Z_e of seawater in the circuit. At this time, the new inductance values L'_1 and L'_2 of the coil can be equivalent to

$$L'_p = L_p \parallel L_e, L'_s = L_s \parallel L_e \tag{10}$$

The equivalent transfer model can be expressed as follows:

$$U_{in} = \left(j\omega L'_p + \frac{1}{j\omega C_e}\right) i_p + i'_p(R_{Lp} + R_e) - j\omega M' i_s \tag{11}$$

$$j\omega M' i_p = U_{out} + \left(j\omega L'_s + \frac{1}{j\omega C_e}\right) i_s + i'_s(R_{Ls} + R_e) \tag{12}$$

For convenience of analysis, the sum of the equivalent resistance of seawater and the internal resistance of the coil is equivalent to the new internal resistance of the coil, and the above formula can be simplified as folllows:

$$U_{in} = j\omega\left(L'_p - \frac{1}{\omega^2 C_e}\right) i_p + i'_p R' - j\omega M' i_s \tag{13}$$

$$j\omega M' i_p = U_{out} + j\omega\left(L'_s - \frac{1}{\omega^2 C_e}\right) i_s + i'_s R' \tag{14}$$

Compared with the equivalent transport model in air, the equivalent transport model in seawater has the same expression form, but the parameter size has changed. Therefore, in the analysis process of underwater wireless power transmission, the analysis of seawater medium characteristics can be added based on the theory of wireless power transmission in the air.

In the process of underwater power transmission, the power loss generated on the circuit and coil is the same as that in air, and what is added is the eddy current loss generated by the alternating magnetic field in seawater. The output power of the system can be expressed as the difference between the output power in the air environment and the eddy current loss power:

$$P_{output\_seawater} = P_{in\_total} - P_{circuits} - P_{coils} - P_{eddy} = P_{output\_air} - P_{eddy} \tag{15}$$

Referring to the expression of transmission efficiency in air environment, the transmission efficiency in seawater environment can be expressed as follows:

$$\eta_{seawater} = \frac{P_{output\_air} - P_{eddy}}{P_{in\_total}} \times 100\% = \eta_{air} - \frac{P_{eddy}}{P_{in\_total}} \times 100\% \tag{16}$$

It can be seen that the transmission efficiency in seawater is determined by the transmission efficiency in air and the eddy current loss generated by seawater. In the previous section, the transmission efficiency of the air system was analyzed, and the eddy current loss will be calculated below.

When the base station wirelessly charges underwater equipment, the wireless power transfer system is installed in a cylindrical sealed docking device, and the seawater gap between the two couplers is close to the shape of a cylinder [15]. The seawater gap between the magnetic coupler is equivalent to the cylindrical area shown in Figure 6, the centers of the two circular coils with the gap distance h are on the same axis, and the currents flowing through the transmitting coil and the receiving coil are I_p and I_s, respectively. Under this model, the magnetic field H_z generated in seawater satisfies the eddy current field equation:

$$j\omega\mu H_z = \frac{\partial^2 H_z}{\partial x^2} = k^2 Hz \tag{17}$$

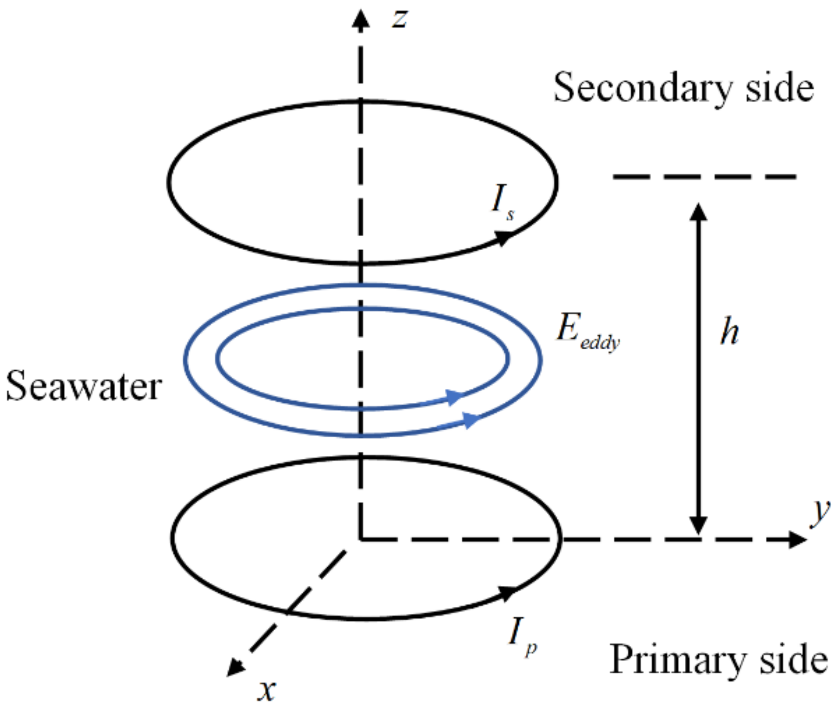

Figure 6. Schematic diagram of eddy current loss.

The power loss generated by the eddy current in the cylinder area between the two coils can be approximated by Formula (18):

$$P_{eddy} \approx \frac{2\omega^2 |B_{zav}|^2 \pi h r^4 \sigma}{3} \tag{18}$$

Among them, ω is the operating angular frequency of the system; h is the transmission distance between the two coils; r is the radius of the coil; B_{zav} is the average value of the magnetic induction along the section, which can be expressed by Formula (19):

$$B_{zav} = \frac{B_o}{rk} \sinh kr \tag{19}$$

Let the number of turns of the coil be n, and B_o can be estimated by adding the magnetic induction intensity vectors generated by the currents I_1 and I_2 flowing in the two coils:

$$B_1 = \frac{\mu n I_1}{2r}, B_2 = \frac{\mu n I_2}{2r}, B_o = \sqrt{B_1^2 + B_2^2} \tag{20}$$

According to Formulas (18)–(20) to simulate the eddy current loss between the coils of the magnetic coupler, let the coil radius $r = 5$ cm and the number of turns $n = 15$.

Figure 7a shows the variation in the eddy current loss generated by the coupler in seawater with the system frequency under different transmission distances when the coil currents at the transmitter and receiver are equal ($I_1 = I_2 = 5A$). It can be seen that the eddy current loss is positively correlated with the transmission distance between the two coils, and the larger the transmission distance, the higher the power loss will be. At the same time, as the system frequency increases, the eddy current loss increases rapidly at different transmission distances. When the system frequency exceeds about 100 kHz, the eddy current loss caused by all transmission distances will increase exponentially.

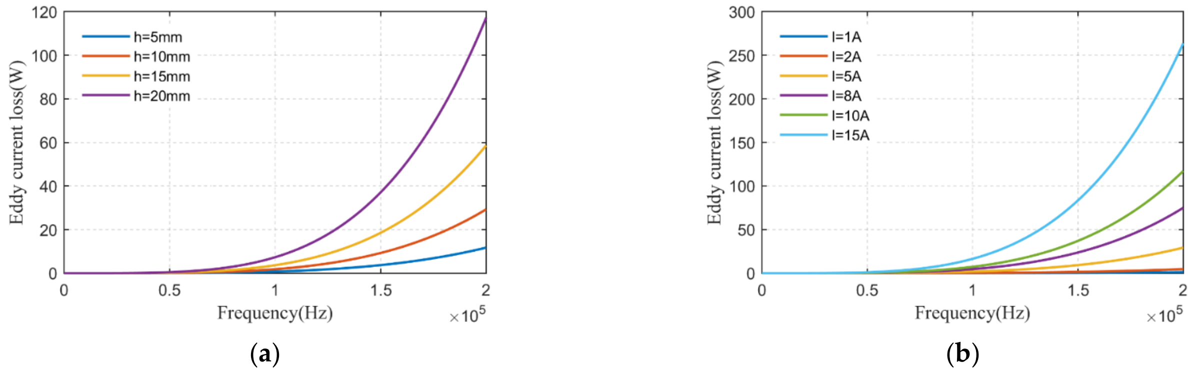

Figure 7. Trends of eddy current loss variation with system parameters: (**a**) eddy current loss versus frequency for different transmission distances; (**b**) eddy current loss versus frequency for different coil currents.

Figure 7b shows that the eddy current loss changes with the system frequency when the transmission distance between the coupler coils is fixed ($h = 5$ mm) and the coil current ($I_1 = I_2 = I$) changes. It can be seen that the eddy current loss is positively correlated with the magnitude of the current flowing in the coil; the greater the current, the greater the intensity of the excited electric field and the higher the power loss. When the current in the coil $I \leq 5A$, the eddy current loss will be higher than before when the system frequency exceeds 150 kHz, and the maximum power loss will not exceed 30 W when the system frequency is within 200 kHz. When the coil current $I > 5A$, the eddy current loss doubles when the system frequency is close to 100 kHz. When the coil current $I = 15A$, the corresponding power loss curve is significantly higher than the other curves. When the system frequency is 150 kHz, the theoretical value of eddy current loss reaches about 80 W.

The above analysis shows that the distance between the coupler and the operating current of the coil will have a greater impact on the eddy current loss. In the actual operation of the system, in order to reduce the power loss caused by eddy currents, excessive coupler spacing should be avoided. In the analysis of the mutual inductance of couplers mentioned above, excessively high spacing will reduce the mutual inductance between couplers. On the other hand, a higher coil current will generate a stronger alternating magnetic field, resulting in a higher transmission capacity. However, at the same time, it will also generate a higher eddy current loss, so this parameter should be set reasonably. Combined with the calculation method of the transmission efficiency in the air and the calculation method of the eddy current loss, the transmission efficiency under different resonance frequencies and load resistance values in the seawater is calculated as a reference for selecting the optimal parameters. The calculation results of transmission efficiency in seawater are shown in Figure 8.

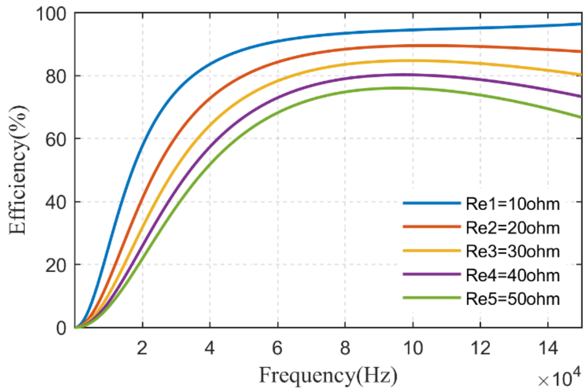

Figure 8. Transmission efficiency versus frequency for different loads in seawater.

Generally speaking, the transmission efficiency of the system in seawater will increase with the resonance frequency and then decrease slowly. The efficiency decrease is mainly due to the joint action of circuit power loss and seawater eddy current loss at high frequencies. Under different loads, the resonant frequency points for the system to achieve optimal transmission efficiency are different. It can be seen from Figure 8 that when the resonant frequency is between 80 kHz and 120 kHz, the transmission efficiency under each load reaches the maximum value. According to the output power level and hardware circuit design experience, this paper chooses 85 kHz as the resonant frequency of the system, which can achieve higher transmission efficiency under different loads.

4. Magnetic Coupler Structure Design and Optimization

The coupler coils for wireless power transmission can be divided into planar coils and coaxial solenoid coils. The magnetic field distribution of the planar coil is concentrated, the relative area between the coils is relatively large, the transmission capacity is strong, and the thickness of the coil structure is thin, which can be miniaturized by design [16]. The internal magnetic field of the coaxial solenoid coil is strong, the external magnetic field is weak, the transmission distance is short, the coupling coefficient is relatively high, and the relative rotation between the two coils is allowed. It is suitable for the wireless power transmission system where the transmitter and the receiver generate relative rotation. The application in this paper requires stronger transmission capacity and distance. It does not need to consider the problem of rotation between devices, so the planar coil solution is selected. Additionally, 200 strands of Litz wire with a diameter of 2 mm are selected as the coil wire for coil winding. It is not significantly affected by the skin effect and proximity effect, and the current flow capacity reaches 7.85 A; the withstand voltage is 4000 V. It can be safely used under the system requirements of this paper.

The design of the magnetic core is related to many factors, such as the equipment's docking structure, the coupling mechanism's volume, and the transmission power requirements. This paper adopts a pot-type magnetic core structure for underwater application scenarios, which can facilitate the underwater docking and fixing of the coupling mechanism. This structure has good electromagnetic shielding characteristics, can reduce magnetic flux leakage, and improve the coupling coefficient between coils. The magnetic core material adopts PC95 manganese zinc ferrite, which has the characteristics of high magnetic permeability, high resistivity, and low hysteresis loss. A 3D structure diagram of the magnetic core is shown in Figure 9a. Establish the 3D model of the coupler core and coil in the finite element software as shown in Figure 9b and analyze the performance of the coupler. Select eddy current field as the solver type, ferrite as the core material, copper as the coil material, vacuum as the peripheral region material, and Balloon condition as the boundary condition. In order to simulate the actual effect produced by the Litz line, the coil winding type is Stranded, and a 125 ampere-turn excitation is added to the transmitter coil. The grid adopts self-adaptive subdivision, and the grid length is selected as medium-length. The front view and top view of the magnetic induction of the coupler are shown in Figure 10a,b, respectively.

According to the simulation results, it can be seen that, due to the closed structure of the pot core, the spatial magnetic field is mainly distributed inside the coupler and concentrated on the central axis of the coil winding at the transmitter and the receiver. Therefore, the magnetic field will not cause electromagnetic interference to external equipment. When the two magnetic cores are entirely aligned and the air gap is small, the space leakage magnetic flux is minimal, and the coupler has a high transmission capacity. In the case of inputting a significant excitation, the magnetic core does not reach magnetic saturation, which meets the power transmission requirements of this paper.

(a) (b)

Figure 9. Models of coupler cores: (**a**) 3D model diagram of magnetic core; (**b**) coupler 3D model diagram.

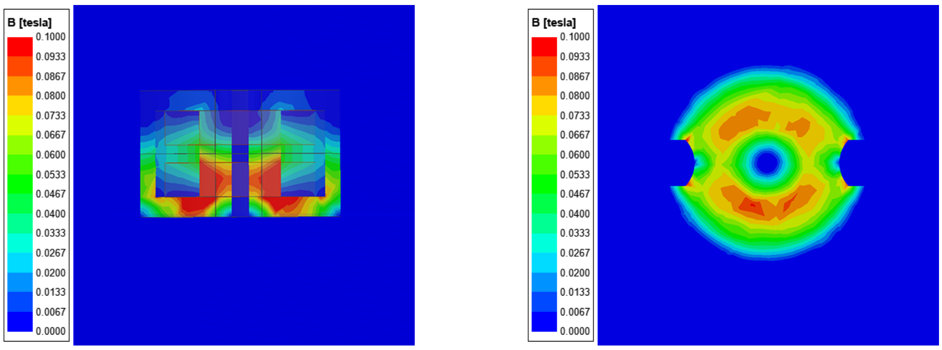

(a) (b)

Figure 10. Finite element simulation results: (**a**) front view of coupler magnetic induction intensity distribution; (**b**) top view of coupler magnetic induction intensity distribution.

When the relative positions of the two ends of the coupler change, the coupler's mutual inductance and coupling coefficient will change. Figure 11a–c show how the mutual inductance and coupling coefficient change with the misalignment distance and angle when the coupler is misaligned laterally, vertically, and angularly. Both show a monotonous downward trend. The coupler has a high tolerance for lateral misalignment. When a small distance of lateral misalignment occurs, the coupling coefficient and mutual inductance will not change in an extensive range, but it is more sensitive to vertical and angular misalignment. A small range of misalignment will cause a significant drop in the coupling coefficient and mutual inductance.

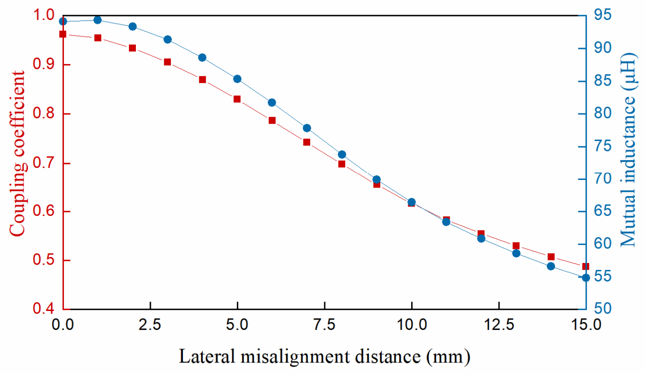

(a)

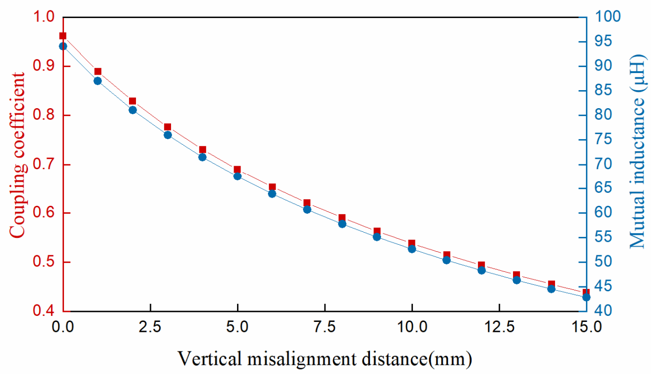

(b)

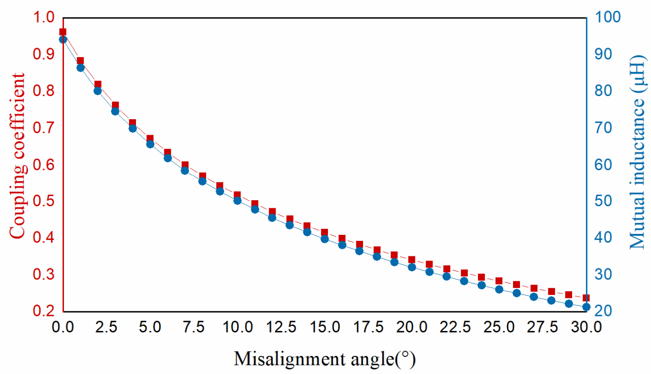

(c)

Figure 11. Effects of misalignment in different directions on coupling coefficient and mutual inductance: (**a**) coupling coefficient and mutual inductance versus lateral misalignment distance; (**b**) coupling coefficient and mutual inductance versus vertical misalignment distance; (**c**) coupling coefficient and mutual inductance versus misalignment angle.

5. Experimental Verification

According to the design plan in this paper, the prototype and experimental platform obtained after fabrication are shown in Figure 12. In actual underwater applications, the circuit board needs to be installed in a cylindrical titanium alloy pressure-resistant chamber. In order to facilitate installation and save space, the circuit board is designed as a circular plate with a diameter of 15 cm, and through holes are reserved around it for fixing. The system design parameters are shown in Table 2.

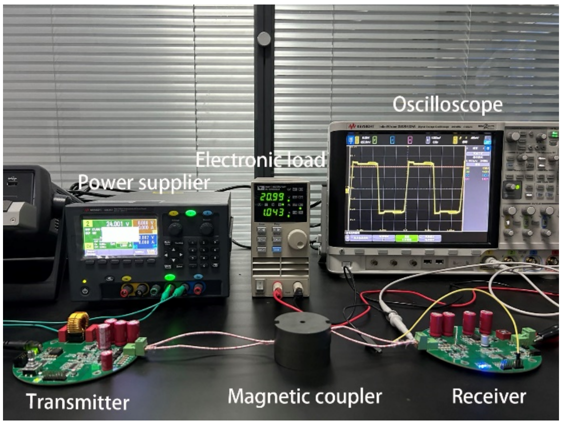

Figure 12. Schemes follow the same formatting.

Table 2. System Parameters.

Description	Parameter	Value
Input dc voltage	U_d/V	24
Self-inductance of the transmitting coil	$L_p/\mu H$	34.26
Self-inductance of the receiving coil	$L_s/\mu H$	34.29
Internal resistance of the transmitting coil	R_{Lp}/Ω	0.1
Internal resistance of the receiving coil	R_{Ls}/Ω	0.1
Series compensation capacitor of the transmitting coil	$C_p/\mu F$	0.1
Series compensation capacitor of the receiving coil	$C_s/\mu F$	0.1
Turns of the coil	n	15
Radius of the coil	r/mm	24.8
Distance between the coils	h/mm	1
Resonant frequency	f_0/kHz	85

In the design of the prototype, the transmitter uses the drive chip IRS2008 and high-speed MOSFETs to form an inverter and drive circuit, and the control signal is sent by the microcontroller STM32F103. The receiver uses a synchronous rectification chip IR1161LPBF and MOSFETs to form a synchronous rectification circuit, which replaces the traditional diode rectification circuit and reduces the power loss caused by the voltage drop on the diode. The input DC voltage is fixed at 24 V, the electronic load ITECH IT8211 is set to CR mode, and the load is fixed at 20 ohm. The Keysight DSOX4024A oscilloscope is used to capture the voltage waveforms on the switches and couplers at the transmitter and receiver. The output signal waveform of two drive circuits of one half-bridge inverter circuit is shown in Figure 13a. It can be seen that the signals in the same half of the inverter circuit are opposite to each other, and a certain dead time is left to avoid simultaneous conduction of the upper and lower switch tubes and short-circuit damage to the circuit. The waveforms of the gate–source voltage V_{GS} and drain–source voltage V_{DS} of the power switch tube of the inverter circuit are shown in Figure 13b. Among them, channel one of the oscilloscope is the waveform of the switch tube V_{GS}, and channel two is the waveform of the switch tube V_{DS}. It can be seen that, before the gate–source voltage of the switch tube V_{GS} reaches the turn-on threshold, the drain–source voltage V_{DS} drops to 0 V, which indicates that the switch tube works in the ZVS soft switching state; the switching loss is slight, which is beneficial for improving the working efficiency of the converter. The voltage waveform of the transmitting coil and the voltage waveform of the receiving coil are shown in Figure 13c,d. It can be seen that both are stable AC square waves. The coil at the receiver induces energy to form a stable voltage, and the system works normally.

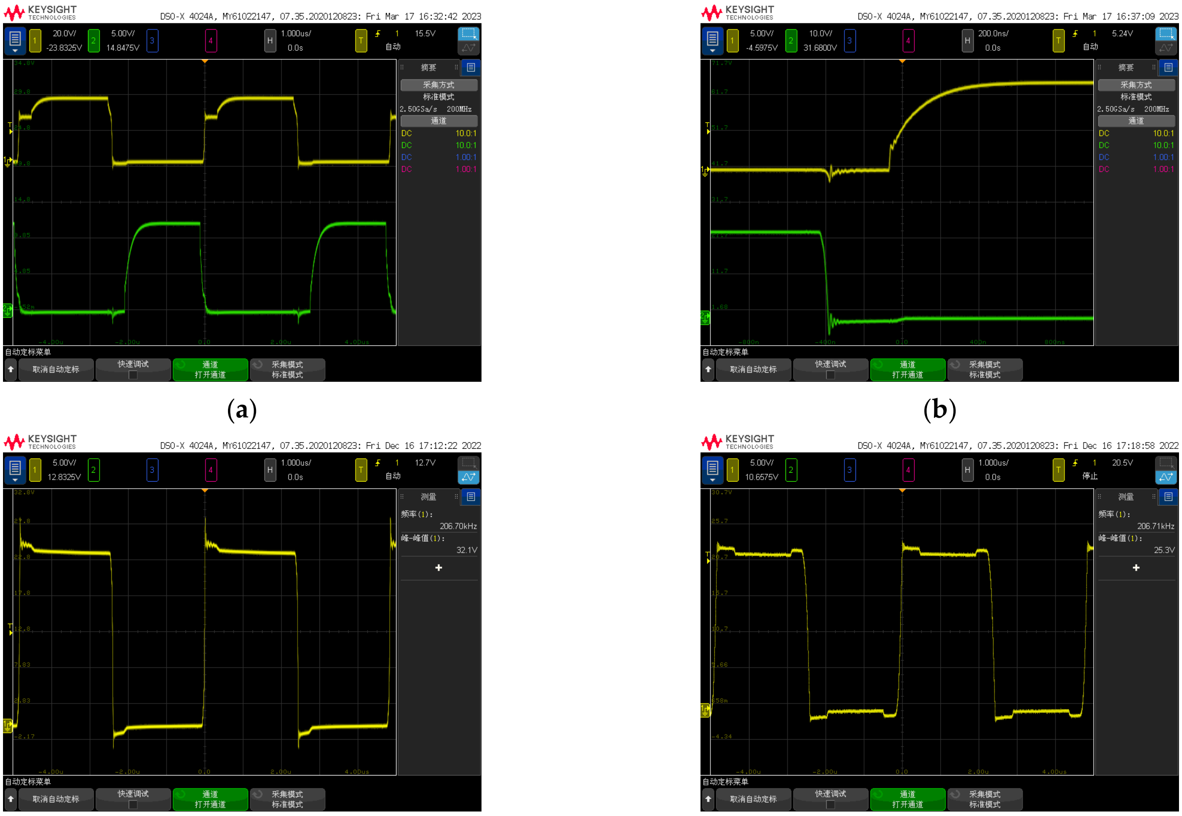

(**a**) (**b**) (**c**) (**d**)

Figure 13. Waveform diagram of the transmitter and receiver: (**a**) output waveform of the drive circuit; (**b**) V_{GS} and V_{DS} waveforms of the switching tube; (**c**) transmitting coil voltage waveform; (**d**) receiving coil voltage waveform.

The transmission capability of the system is tested in an air environment. The theoretical value of performance under the above system parameters can be obtained from the calculation method in Section 3. The access load resistance is 20 ohm; the comparison results of the experimental measurement and theoretical values of the system output power and transmission efficiency at different operating frequencies are shown in Figure 14a,b. The experimental results are basically close to the theoretical values, and the trends of the curves are consistent, which verifies the correctness of the theoretical model. The output power and transmission efficiency increase first and then decrease with the operating frequency, reaching the highest value near the system resonance frequency. The transmission power reaches 60 W around 85 kHz, and the transmission efficiency reaches 85%.

Under the condition that the operating frequency is equal to the system resonance frequency of 85 kHz, the comparison results of the experimental measurement and theoretical values of the system output power and transmission efficiency under different load resistance values are shown in Figure 14c,d. It can be seen that the experimental results are basically close to the theoretical values, and the trend of change is consistent. The output power of the system increases with the load resistance, while the changing trend of the transmission efficiency is opposite. The two cannot be optimal simultaneously, which aligns with the theoretical analysis results above. The reason for the difference between the actual output power and the theoretical value under a large load may be the measurement error on the one hand, and the increase in the loss of the device at high temperature on the other hand may cause the actual output power to decrease. In practical applications, the optimal load value can be selected according to the power demand, and the load value can be reduced to improve the system transmission efficiency to meet the system power demand.

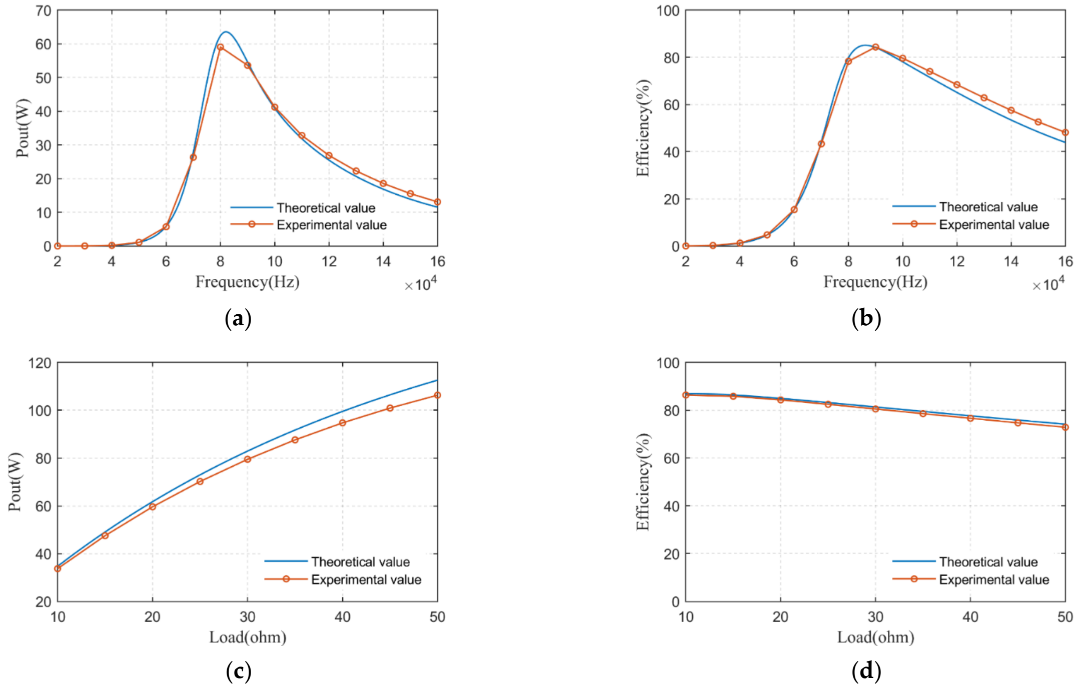

Figure 14. Experimental results in air: (**a**) output power corresponding to different operating frequencies in air environment; (**b**) transmission efficiency corresponding to different operating frequencies in air environment; (**c**) output power corresponding to different loads in air environment; (**d**) transmission efficiency corresponding to different loads in air environment.

The coupler coil was placed in a 3.5% sodium chloride solution for the simulated seawater environment transmission experiment. The experimental environment is shown in Figure 15. The system access load resistance is 20 ohm. Change the system operating frequency. Measure and calculate the output power comparison curve between the seawater and the air, as shown in Figure 16a, and the transmission efficiency comparison curve between the seawater and the air is shown in Figure 16b; the eddy current loss curve shown in Figure 16c. It can be seen that when the frequency is lower than 100 kHz, the output power and transmission efficiency of the system in the seawater are very close to those in the air, and the eddy current loss is at a very low level. When the frequency exceeds 100 kHz, the difference between the output power and transmission efficiency measured in the seawater and the experimental results in the air begins to increase gradually with the frequency increase, and the value of the eddy current loss increases rapidly.

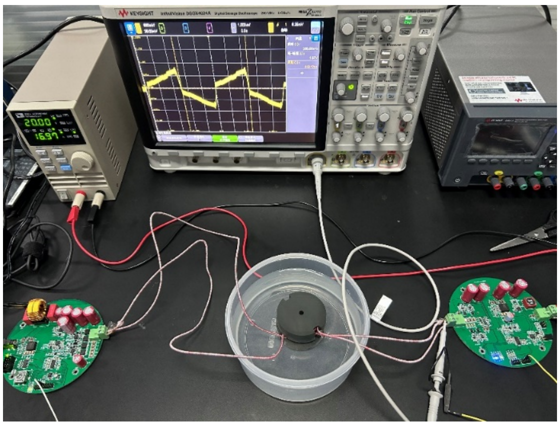

Figure 15. Simulated seawater environment experiment.

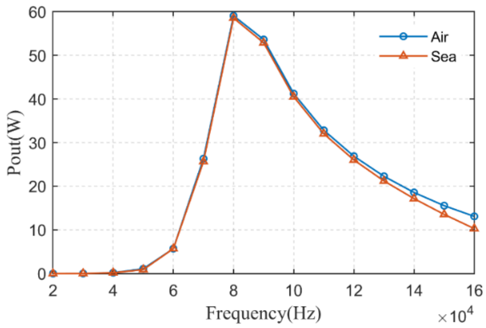

(**a**)

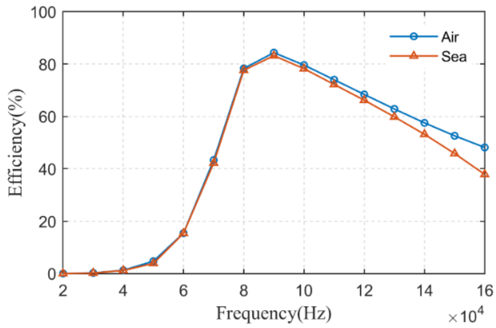

(**b**)

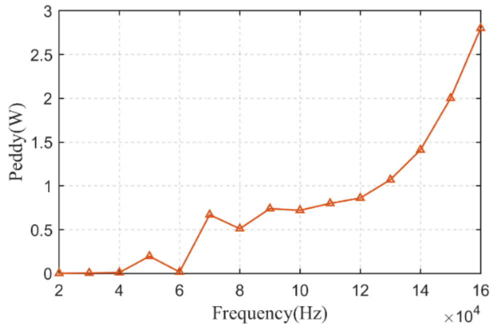

(**c**)

Figure 16. Experimental results in seawater: (**a**) output power corresponding to different operating frequencies in seawater environment; (**b**) transmission efficiency corresponding to different operating frequencies in seawater environment; (**c**) eddy current loss corresponding to different operating frequencies in seawater environment.

Summarizing the experimental results in Figure 16, it can be concluded that, for the system in this paper, the eddy current loss increases significantly when the frequency exceeds 100 kHz. The value of the eddy current loss is very small near the system resonance frequency of 85 kHz. The influence of the seawater on the system's transmission performance is insignificant. The transmission efficiency reaches about 83%, showing that the parameter setting in this paper is reasonable and can still maintain a high transmission efficiency in the seawater. Table 3 shows the comparison results between the proposed system and some previous underwater wireless power transfer systems. Since there are few studies on small and medium power systems (less than 100 W) in the existing literature, systems with higher power levels are selected for comparison. The transmission efficiency of the system in this paper has certain advantages in small and medium power systems.

Table 3. Comparison with previous underwater wireless power transfer systems.

Reference	[9]	[5]	[13]	**This Paper**
Magnetic coupler structure	Linear coaxial winding transformer	Arc-shaped improved EE core	Cylindrical barrel	Pot-type magnetic core
Power level	240 W	Unknown	100 W	57 W
Efficiency	70%	82%	67%	83%

6. Conclusions and Prospects

This paper proposes a wireless power transfer system suitable for underwater working environment. The circuit structure of the system based on SS type compensation network has been designed, and the circuit modeling analysis results show that it can realize constant current output without load interference and that it has certain dislocation tolerance. The operational characteristics of the system have been analyzed, and the influence of the resonant frequency, load resistance, and coupling coefficient on the system's output capacity in the air has been studied. The system transmission model and eddy current loss model in seawater were proposed; the eddy current loss generated by transmission in seawater is calculated according to the eddy current field equation, and the calculation method of transmission efficiency in seawater is determined in combination with the transmission efficiency formula in air. The calculation results show that when the coil current is less than or equal to 5 A, the eddy current loss is slight when the operating frequency is within 150 kHz, and the eddy current loss will increase significantly when the frequency exceeds 150 kHz. A coupler suitable for loading underwater equipment has been designed, and the finite element simulation results show that it has a certain transmission capability and good electromagnetic shielding capability. A prototype was developed according to the design plan, and the experimental results verified the feasibility and correctness of the theoretical plan. In the air environment, the transmission power reached 60 W at around 85 kHz, and the transmission efficiency reached 85%. In the simulated seawater environment, the output power reaches about 57 W at the same operating frequency, and the transmission efficiency reaches 83%. In future work, the packaging of the wireless power transmission system will be designed. The system packaging needs to complete the alignment of the coil before the power transmission, the release and exit after the power transmission, etc. During the design process, sealing, pressure resistance, corrosion resistance, and other aspects will be studied. The packaged system can be used in actual underwater operations with base stations, underwater vehicles, and other equipment.

Author Contributions: Conceptualization, S.Z. and T.L.; methodology, T.L.; investigation, T.L.; visualization, T.L.; writing—original draft preparation, T.L.; writing—review and editing, S.Z.; supervision, S.Z.; project administration, S.Z.; funding acquisition, S.Z. All authors have read and agreed to the published version of the manuscript.

Funding: This research was funded by State Key Laboratory of Tropical Oceanography, South China Sea Institute of Oceanology, Chinese Academy of Sciences (Project No. LTO 2207); Natural Science Foundation of China (No. 51809255): Research on tracking strategy of ocean cold eddy-upwelling with AUVs.

Institutional Review Board Statement: Not applicable.

Informed Consent Statement: Not applicable.

Data Availability Statement: The data presented in this study are all included in this article.

Acknowledgments: The authors would like to thank the reviewers for their careful work.

Conflicts of Interest: The authors declare no conflict of interest.

References

1. Teeneti, C.R.; Truscott, T.T.; Beal, D.N.; Pantic, Z. Review of Wireless Charging Systems for Autonomous Underwater Vehicles. *IEEE J. Ocean. Eng.* **2021**, *46*, 68–87. [CrossRef]
2. Wang, D.; Cui, S.; Zhang, J.; Bie, Z.; Song, K.; Zhu, C. A Novel Arc-Shaped Lightweight Magnetic Coupler for AUV Wireless Power Transfer. *IEEE Trans. Ind. Appl.* **2022**, *58*, 1315–1329. [CrossRef]
3. Pyle, D.; Granger, R.; Geoghegan, B.; Lindman, R.; Smith, J. Leveraging a Large UUV Platform with a Docking Station to Enable Forward Basing and Persistence for Light Weight AUVs. In Proceedings of the 2012 Oceans, Hampton Roads, VA, USA, 14–19 October 2012; pp. 1–8.
4. Shi, J.; Li, D.; Yang, C. Design and Analysis of an Underwater Inductive Coupling Power Transfer System for Autonomous Underwater Vehicle Docking Applications. *J. Zhejiang Univ.—Sci. C* **2014**, *15*, 51–62. [CrossRef]
5. Yan, Z.; Zhang, K.; Wen, H.; Song, B. Research on Characteristics of Contactless Power Transmission Device for Autonomous Underwater Vehicle. In Proceedings of the OCEANS 2016—Shanghai, Shanghai, China, 10–13 April 2016; pp. 1–5.
6. Li, G.; Zhang, S. The Hydrodynamic Coefficient Analysis and Motion Control of the Lingyun Moveable Lander. *Geofluids* **2021**, *2021*, 3708594. [CrossRef]
7. Tamura, M.; Murai, K.; Matsumoto, M. Design of Conductive Coupler for Underwater Wireless Power and Data Transfer. *IEEE Trans. Microw. Theory Tech.* **2021**, *69*, 1161–1175. [CrossRef]
8. Yoshioka, D.; Sakamoto, H.; Ishihara, Y.; Matsumoto, T.; Timischl, F. Power Feeding and Data-Transmission System Using Magnetic Coupling for an Ocean Observation Mooring Buoy. *IEEE Trans. Magn.* **2007**, *43*, 2663–2665. [CrossRef]

9. McGinnis, T.; Henze, C.P.; Conroy, K. Inductive Power System for Autonomous Underwater Vehicles. In Proceedings of the OCEANS 2007, Vancouver, BC, Canada, 29 September–4 October 2007; pp. 1–5.
10. Stankiewicz, J.M. Analysis of the Influence of the Skin Effect on the Efficiency and Power of the Receiver in the Periodic WPT System. *Energies* **2023**, *16*, 2009. [CrossRef]
11. Wang, J.; Song, B.; Wang, Y. A Method to Reduce Eddy Current Loss of Underwater Wireless Power Transmission by Current Control. *Appl. Sci.* **2022**, *12*, 2435. [CrossRef]
12. Zhou, J.; Li, D.; Chen, Y. Frequency Selection of an Inductive Contactless Power Transmission System for Ocean Observing. *Ocean. Eng.* **2013**, *60*, 175–185. [CrossRef]
13. Zhang, K.-H.; Yan, L.-B.; Yan, Z.-C.; Wen, H.-B.; Song, B.-W. Modeling and analysis of eddy-current loss of underwater contact-less power transmission system based on magnetic coupled resonance. *Acta Phys. Sin.* **2016**, *65*, 048401. [CrossRef]
14. Askari, A.; Stark, R.; Curran, J.; Rule, D.; Lin, K. Underwater Wireless Power Transfer. In Proceedings of the 2015 IEEE Wireless Power Transfer Conference (WPTC), Boulder, CO, USA, 13–15 May 2015; pp. 1–4.
15. Luo, T.; Zhang, S.; Zhou, F. Research on an Underwater Inductive Coupling Power Transfer Method. In Proceedings of the 2022 IEEE 4th International Conference on Power, Intelligent Computing and Systems (ICPICS), Shenyang, China, 29–31 July 2022; pp. 167–173.
16. Yan, Z.; Zhang, K.; Qiao, L.; Hu, Y.; Song, B. A Multiload Wireless Power Transfer System With Concentrated Magnetic Field for AUV Cluster System. *IEEE Trans. Ind. Appl.* **2022**, *58*, 1307–1314. [CrossRef]